Available online at www.sciencedirect.com
SCIENCE DIRECT®
Composites Science and Technology 65 (2005) 2541–2549
COMPOSITES SCIENCE AND TECHNOLOGY
www.elsevier.com/locate/compscitech

Effect of on-axis tensile loading on shear properties of an orthogonal 3D woven SiC/SiC composite

Toshio Ogasawara [a,*], Takashi Ishikawa [a], Tomohiro Yokozeki [a], Takuya Shiraishi [b,1], Naoyuki Watanabe [b]

[a] Advanced Composite Evaluation Technology Center, Japan Aerospace Exploration Agency (JAXA), Mitaka, Tokyo 181-0015, Japan
[b] Aerospace Systems Department, Tokyo Metropolitan University, Hino, Tokyo 191-0065, Japan

Received 2 June 2005; accepted 2 June 2005
Available online 28 July 2005

Abstract

The present study examines in-plane and out-of-plane shear properties of an orthogonal 3D woven SiC fiber/SiC matrix composite. A composite beam with rectangular cross-section was subjected to a small torsional moment, and the torsional rigidities were measured using an optical lever. Based on the Lekhnitskii's equation (Saint–Venant torsion theory) for a orthotropic material, the in-plane and out-of-plane shear moduli were simultaneously calculated. The estimated in-plane shear modulus agreed with the modulus measured from ±45° off-axis tensile testing. The effect of on-axis (0°/90°) tensile stress on the shear stiffness properties was also investigated by the repeated torsional tests after step-wise tensile loading. Both in-plane and out-of-plane shear moduli decreased by about 50% with increasing the on-axis tensile stress, and it is mainly due to the transverse crack propagation in 90° fiber bundles and matrix cracking in 0° fiber bundles. It was demonstrated that the torsional test is an effective method to estimate out-of-plane shear modulus of ceramic matrix composites, because a thick specimen is not required.

Keywords: Ceramic matrix composites; Matrix cracking; Transverse cracking; Finite element analysis

1. Introduction

It is now well understood that continuous fiber ceramic matrix composites (CMCs) exhibit nonlinear stress–strain behavior under tensile loading as a result of multiple microcracking and fiber fragmentation. An overview of CMC mechanical properties has been provided by Evans and Zok [1]. For unidirectional CMCs, the change in stiffness due to multiple matrix cracking has been estimated by elastic analysis based on the Lame problem [2], and shear-lag analysis [3]. In cross-ply composites, this change also involves initial cracking in the transverse (90°) plies as tunneling cracks [4–7]. Subsequently, transverse cracks penetrate the longitudinal plies as the load is increased. Based on the energy criterion and finite element analysis, transverse crack propagation in cross-ply brittle matrix composites has been analyzed [6,7]. Shear-lag analysis is often used to estimate transverse crack propagation within polymer matrix composites [8], and this method has also been applied to an orthogonal 3D woven CMC as well as cross-ply CMCs [9].

The effect of transverse crack on shear stiffness degradation has been investigated for polymer matrix composites. For example, Kobayashi et al. [10] investigated the effect of on-axis tensile loading on degradation of in-plane and out-of-plane shear moduli of cross-ply carbon fiber/epoxy composites. The experimental results

* Corresponding author. Tel.: +81 422 40 3561; fax: +81 422 40 3549.
E-mail address: ogasat@chofu.jaxa.jp (T. Ogasawara).
[1] Former graduate student, Currently in Mitsubishi Space Software Co., Ltd., Kanagawa, Japan.

0266-3538/$ - see front matter © 2005 Elsevier Ltd. All rights reserved.
doi:10.1016/j.compscitech.2005.06.003

were compared with the numerical results based on Tsai–Daniel model [11], Hashin model [12], and Gudmundson–Zang model [13], and conservative stiffness degradation as a function of transverse crack density was predicted by these models.

Some researchers experimentally investigated the degradation of in-plane shear modulus in CMCs by off-axis tensile test and V-notched shear (Iosipescu) test [14,15], and the effect of in-plane shear stress on in-plane shear stiffness degradation has been understood. However, the effect of on-axis loading on the in-plane and out-of-plane shear properties of CMCs have not been revealed yet.

For evaluating the effect of on-axis loading on shear properties, the shear modulus of a composite which has microscopic damages caused by on-axis tensile stress should be measured. However, it is difficult to make *thick* CMC specimens because of difficulty in processing. Standard test methods such as rail-shear method (ASTM-D4255), off-axis tensile test method (ASTM D3518), V-notched shear (Iosipescu) method (ASTM C1292) are not applicable for measuring out-of-plane shear modulus of *thin* CMC specimens.

A unique test method for measuring out-of plane shear modulus has been provided by Ishikawa et al. [16]. They applied a torsional test for estimating out-of plane shear modulus of a unidirectional carbon fiber/epoxy composite based on Lekhnitskii's torsion theory [17]. Tsai et al. also presented a closed-form solution for a composite laminate under torsion in terms of the lamination geometry, and the experimental methodology to determine the three principal shear moduli by measuring surface and edge strains in twisted prismatic coupons [18]. The torsional test is useful to estimate out of plane shear properties, because a thick specimen is not required for the experiment.

In this study, the in-plane and out-of-plane shear properties of an orthogonal 3D woven SiC fiber/SiC matrix composite were evaluated by torsional test of a rectangular cross-section beam. The experimental results were compared with numerical results by finite element analysis (FEA). Furthermore, the effect of on-axis tensile loading on shear modulus degradation of the SiC/SiC composite was also examined.

2. Torsional test methodology

Based on Lekhnitskii's torsion theory for an orthotropic material, Swanson established a torsion theory for composite laminated rectangular rods [19]. However, it is difficult to expand this theory for an orthogonal 3D woven composite. Therefore, Lekhnitskii's torsion theory is directly applied, assuming an orthogonal 3D woven composite as a uniform orthotropic material.

A schematic drawing of a torsion beam is shown in Fig. 1. A specimen consists of a rectangular cross-section beam with dimensions b (width) by h (thickness) in y and z directions, with L (length) in x direction. The coordinate x is parallel to a material axis. For an orthotropic material twisted about an axis parallel to the material direction (x direction) with torsional moment M_t, the torsional rigidity GJ ($=M_t/\omega$) is given by [17]:

$$GJ = G_{xy}\beta(c)bh^3,$$
$$\beta(c) = \frac{32c^2}{\pi^4}\sum_{k=1,3,5\ldots}^{\infty}\left\{1 - \frac{2c}{k\pi}\tanh\left(\frac{k\pi}{2c}\right)\right\},$$
$$c = \frac{b}{h}\sqrt{\frac{G_{zx}}{G_{xy}}}, \tag{1}$$

where ω is a twist angle per unit length, G_{xy} and G_{zx} are in-plane and out-of-plane shear moduli. As this equation is based on Saint–Venant torsion, so-called "warping effects" are neglected.

Ishikawa et al. [16] investigated the effect of warping-torsion on the torsional rigidity of a unidirectional composite beam, and revealed that torsional rigidity increases under the warping torsion. For an actual experiment, specimen grip areas shown in Fig. 1 are constrained for applying torsion moment and for fixing specimen with a fixture. Therefore, the effect of warping on torsional rigidity was preliminarily investigated by finite element analysis (FEA). A commercial FEA code ABAQUS was used for the calculation.

The numerical results under the condition of $L/H = 26.7$, and $G_{xy}/G_{zx} = 2$ are shown in Fig. 2 for b/h of 1, 2, 4, and 8. ω_n and ω_a are twist angles per length calculated by FEA and Lekhnitskii's torsion theory (Eq. (1)), respectively. While the grip areas are assumed to constrain the warping deformation strictly in the calculation, these boundary conditions are much stricter than those in an actual experiment. The

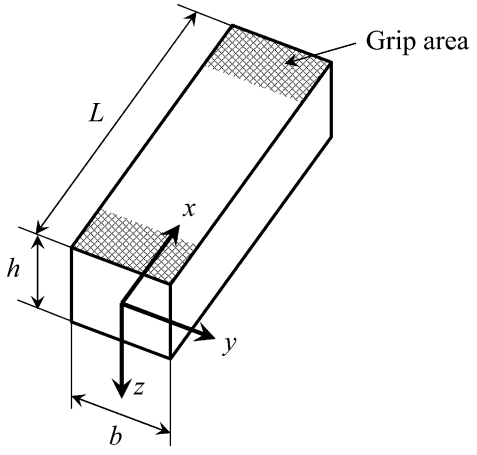

Fig. 1. Specimen configuration and coordinate system for torsional test.

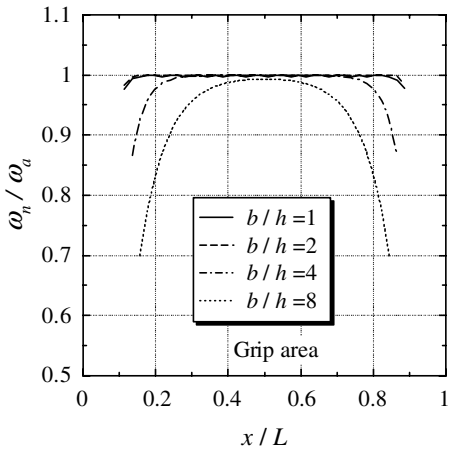

Fig. 2. Effect of cross-section geometry (b/h) on warping torsion ($L/H = 26.7$, $G_{xy}/G_{zx} = 2$, $b/h = 1, 2, 4, 8$). ω_n: twist angle per length calculated from FEA, ω_a: twist angle per length calculated from the Lekhnitskii's equation (Eq. (1)).

numerical results were almost independent on the shear modulus ratio (G_{xy}/G_{zx}) on the numerical results. When $b/h \leqslant 2$, the ω_n/ω_a values are almost unity (0.999–1.000) between 0.3 and 0.7 of x/L. However, the effect of warping becomes more significant with increase in b/h. The numerical result suggests that the effect of warping on torsional rigidity can be neglected under the condition of $b/h < 2$ and $0.25 < x/L < 0.75$.

The shear moduli G_{xy} and G_{zx} are determined by the following procedure. When the specimen width b and thickness h are fixed, the torsional rigidity GJ is represented as a function of G_{xy} and G_{zx} as follows:

$$GJ = f(G_{xy}, G_{zx}). \tag{2}$$

Considering two specimens, 1 and 2, with different rectangular cross-section, the following nonlinear simultaneous equations f_1 and f_2 are obtained:

$$\begin{cases} GJ_1 = f_1(G_{xy}, G_{zx}), \\ GJ_2 = f_2(G_{xy}, G_{zx}). \end{cases} \tag{3}$$

In Eq. (3) GJ_1 and GJ_2 are obtained from torsional experiments. The two equations are solved for G_{xy} and G_{zx} by any numerical methods such as Newton–Raphson method.

3. Experimental procedure

3.1. Materials [9,20]

The composite under investigation contained Tyranno™ Lox-M fibers woven into an orthogonal 3D configuration with fiber volume fractions of 19%, 19%, and 2% in the x, y, and z directions, respectively. Optical micrographs and schematic drawing in Fig. 3 illustrate the fiber architecture of the present composites with each fiber bundle containing 1600 fibers. The composite preform plate ($240 \times 120 \times 6$ mm) was treated at elevated temperature in a CO atmosphere, resulting in the formation of a 10 nm SiO_x-rich layer surrounding an inner 40 nm carbon-rich layer at the fiber surface [20]. The nano-scale carbon-rich layer is believed to result in interphase with desirable properties between the fiber and matrix. Poly-titano-carbosilane was used as the matrix precursor with eight impregnation and pyrolysis cycles, the average composite bulk density was 2.20 g/cm^3. Tensile specimens were machined from the composite plates such that the loading direction was parallel to the y-axis. The specimen surfaces were also ground to a flat finish such that the interlacing loops shown in Fig. 3 were not present in the final specimens. The unit cell size is 3 mm × 3 mm.

3.2. Tensile tests

Both on-axis (0°/90°) and off-axis (±45°) tensile tests were conducted on a servo-hydraulic testing rig (Model 8501, Instron, USA) at room temperature in air using a specimen geometry as shown in Fig. 4(a) Cardboard tabs were bonded to the specimen end regions with the load being applied using hydraulic wedge grips. A clip gauge-type extensometer (gauge length 25 mm; Model 632.11C-20, MTS, USA) was used to measure the longitudinal strain. Transverse strains were measured using

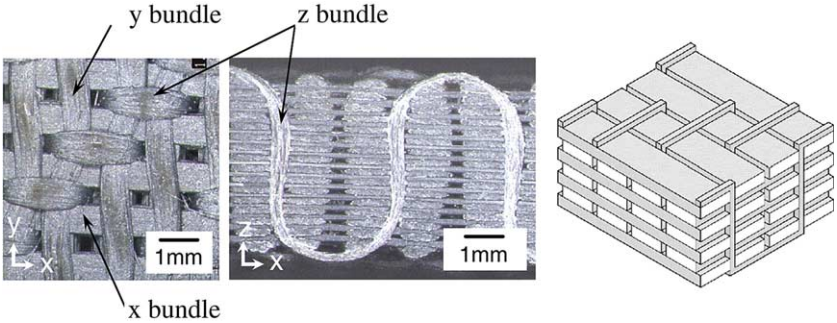

Fig. 3. Optical micrographs and schematic drawing of a SiC/SiC composite illustrating the orthogonal 3D woven fiber architecture.

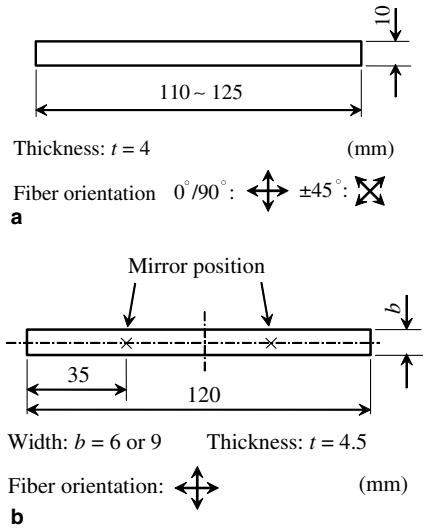

Fig. 4. Specimen configuration and dimensions used for the experiments: (a) tensile test, (b) torsional test.

strain gauges (gauge length 5 mm) which were bonded on both of the specimen surfaces. The displacement rate was 0.5 mm/min.

Matrix cracking characteristics under on-axis loading were investigated for a specimen using the replica film method with surface replicas being taken under load at various stages of the loading cycle.

3.3. Torsional test

Specimen configuration and dimensions used for torsional tests are shown in Fig. 4(b). Two kinds of specimens with different width b ($b = 6$ and 9 mm) were prepared. The thickness, h, was 4.5 mm. Note that the specimen width is 2 or 3 times in the size of a fabric unit cell (3 mm).

Schematic drawings and photograph of torsional test configuration are shown in Figs. 5 and 6, respectively. One end of a specimen was fixed to a base fixture, and a torsion arm was attached at another end. Torsional moment was applied through the torsion arm to the specimen as shown in Figs 5(a) and 6. A weight (F_1) was directly hung at one end of the torsion arm, and a weight (F_2, $F_1 = F_2$) was subjected at another end through the pulley 1. Own weight (w) of the specimen and torsion arm was cancelled using a weight (w) through the pulley 2.

An optical lever system was used for measuring the twist angle of the specimen. An optical lever is a convenient device to magnify a small displacement and thus to make possible an accurate measurement of the displacement. Two small mirrors were put at the point A and B on the specimen upper surface as shown in Figs. 5(a) and 6. He–Ne laser beams were irradiated to the mirrors as shown in Fig. 5(b), and torsion angles θ_A, θ_B were

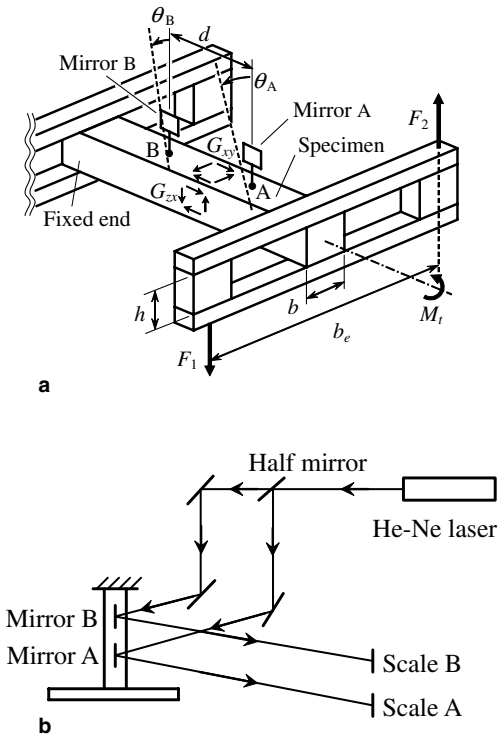

Fig. 5. Schematic configuration of a torsional test: (a) torsional test setting, (b) optical lever system (top view).

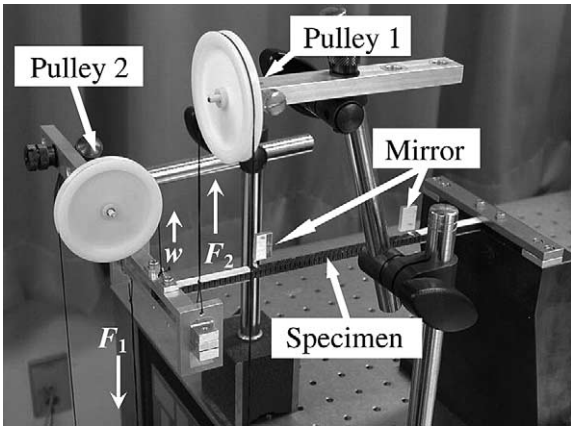

Fig. 6. Photograph showing the torsional test setting.

determined by measuring the distance between the reflected beams. The locations of the mirror points shown in Fig. 5(a) reflect the constraint of $0.25 < x/L < 0.75$ obtained by the FEA simulation. Torsional rigidity GJ is defined as follows:

$$GJ = M_t/\omega, \quad \omega = (\theta_A - \theta_B)/d, \tag{4}$$

where d is the distance between two mirrors (50 mm). Applied torsion moment was between 0.2 and 0.8 N m. It was preliminarily confirmed that microcrack propagation never occur under the torsional moment.

In order to investigate the effect of on-axis loading on shear properties, torsional tests were carried out for the pre-loaded specimen. The specimen was loaded up to peak stress under a constant loading rate of 1 MPa/s, and then unloaded. Consequently, a torsional rigidity was measured by a torsional test. The peak stress was raised step by step, for example, 40, 60, 80 MPa, and so on. When the specimen was broken, the test was finished.

4. Results and discussion

4.1. Monotonic tensile test

Typical stress–strain curves obtained from on-axis (0°/90°) and ±45° off-axis tensile tests are shown in Fig. 7. In-plane shear modulus G_{xy} was estimated from ±45° off-axis stress–strain curves below 30 MPa using the following equation:

$$G_{xy} = \frac{E_{45}}{2(1+\nu_{45})}, \tag{5}$$

where E_{45} and ν_{45} are Young's modulus and Poisson's ratio in ±45° off-axis tensile test.

The Young's modulus E, Poisson's ratio ν , and in-plane shear modulus G_{xy} are summarized in Table 1. Initial Young's modulus E_x, in on-axis (0°/90°), was 126 GPa, which is similar to that in ±45° off-axis testing (118 MPa). The data scatter for three specimens is about 3–6%. However, stress–strain behavior above 30 MPa is much different from each other. It is reported that the stress–strain curves obtained from ±45° off-axis tensile tests did not coincide with those obtained from pure shear tests (Iosipescu configuration) [4,14,15]. This implied that the normal stress σ_x and σ_y as well as shear stress τ_{xy} affected the degradation of shear stiffness G_{xy}.

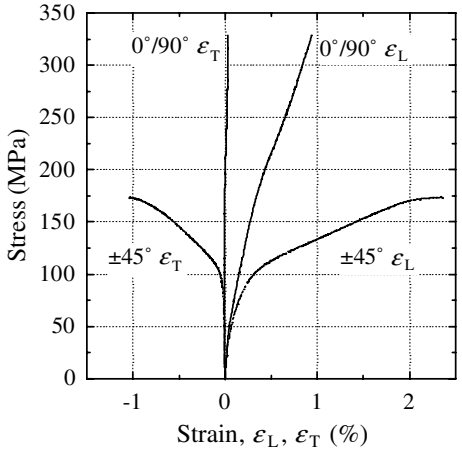

Fig. 7. Typical stress–strain curves obtained from on-axis (0°/90°) and ±45° off-axis tensile tests.

Table 1
Initial elastic moduli obtained from on-axis and ±45° off-axis tensile tests

	Specimen number	E (GPa)	ν	G_{xy} (GPa)
On-axis tensile test	1	126	0.168	
±45° off-axis tensile test	1	114	0.223	46.6
	2	119	0.188	50.1
	3	120	0.210	49.6
	Average	118	0.207	48.8

4.2. Torsional test for pristine specimens

At first, the shear modulus of aluminum alloy (A5052) was measured for verifying the torsional test methodology. Specimens with different rectangular cross-section (thickness 4 mm, width 4 and 6 mm) were used for the experiments. Three specimens for each width were prepared. The shear modulus measured by the torsional test was 27.0 GPa, which agreed with the shear modulus (27.3 GPa) obtained from a tensile test (Young's modulus 72.5 GPa, Poisson's ratio 0.328). Data scattering (coefficient of variation; CV) for aluminum specimens was less than 0.5 %.

Average torsional rigidity GJ obtained from three specimens for each specimen geometry was 4.33 N m^2 for a 6 mm width specimen, and 8.48 N m^2 for a 9 mm width specimen as summarized in Table 2. Data scattering (CV) for composite specimens was about 3–5 % as shown in Tables 1 and 2, and this is much more significant than that for aluminum specimens. The specimen width was only 2 or 3 times in the size of a fabric unit cell (3 mm). This suggests that the scattering in cutting a specimen from a plate affects the experimental results. Therefore, several specimens are required to obtain reliable results. Using Eq. (1), one curve is drawn for one specimen geometry in G_{zx}–G_{xy} plane as shown in Fig. 8, and the intersection of two curves gives the solution of Eq. (1). The shear moduli, G_{xy} and G_{zx}, were determined to be 45.3 and 35.6 GPa, respectively. The measured in-plane shear modulus G_{xy} almost agreed with that measured from the ±45° off-axis tensile test (48.8 GPa).

In G_{zx}–G_{xy} plane, the gradient ($\mathrm{d}G_{zx}/\mathrm{d}G_{xy}$) of a curve increases with increase of b/h, which suggests that the

Table 2
Initial torsional rigidity ($h = 4.5$ mm, $M_t = 0.2$–0.8 N m)

	Specimen number	Width, 6 mm ($b/h = 4/3$)	Width, 9 mm ($b/h = 2$)
Torsional rigidity GJ (N m^2)	1	4.09	8.44
	2	4.50	8.61
	3	4.39	8.39
	Average	4.33	8.48

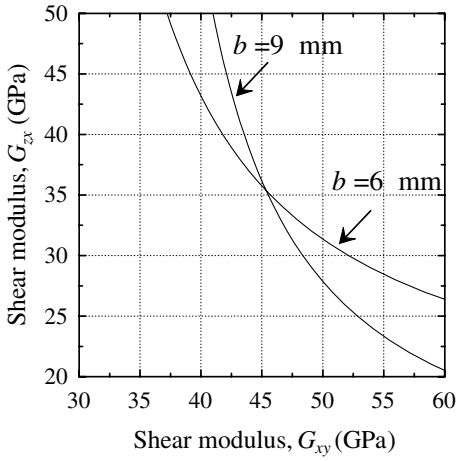

Fig. 8. Estimation of shear moduli G_{xy} and G_{zx} from the torsional test results.

experimental error becomes more significant. Thus, specimen geometry is important to obtain good results in this method. If the in-plane shear modulus is already measured using Iosipescu shear test or 45 off-axis test, the out-of-plane shear modulus can be measured more accurately by this method. If in-plane and out-of-plane shear moduli are unknown, these moduli can be obtained simultaneously. This method only requires small and thin (<3 mm) specimens, and a simple equipment. They are important advantages of this method.

Shear modulus of the pristine composite was estimated by finite element analysis to verify the experimental result. Optical micrograph showing x–z cross-section of the composite is shown in Fig. 9(a). In the pocket region (no fiber bundle region), matrix is separated from the adjacent fiber bundles. Therefore, this region was regarded as entire pore (porosity 10 vol.%). Unit cell was modeled and divided into finite elements as shown in Fig. 9(b). A computer code based on homogenization method was developed and applied for the calculation. Homogenization method is basically a finite element method, and this is effective to deal with periodic structures such as composite materials. Basic methodology of this computer code has been presented elsewhere [21]. Both SiC fiber and SiC matrix were assumed to be isotropic materials with Poisson' ratio of 0.2, and the Young's modulus of SiC fiber was $E_f = 187$ GPa. Young's modulus of SiC matrix, E_m, is an unknown parameter, therefore it was estimated by the parametric study.

Numerical results are shown in Fig. 10. When the Young's modulus of SiC matrix is $E_m = 126$ GPa, the calculated E_x of the composite agrees with the experimental result (126 GPa). Then the calculated shear moduli G_{xy} and G_{zx} are 49.2 and 35.8 GPa, respectively. These values are quite similar to the experimental results obtained from the torsional test, $G_{xy} = 45.3$ GPa, $G_{zx} = 35.6$ GPa.

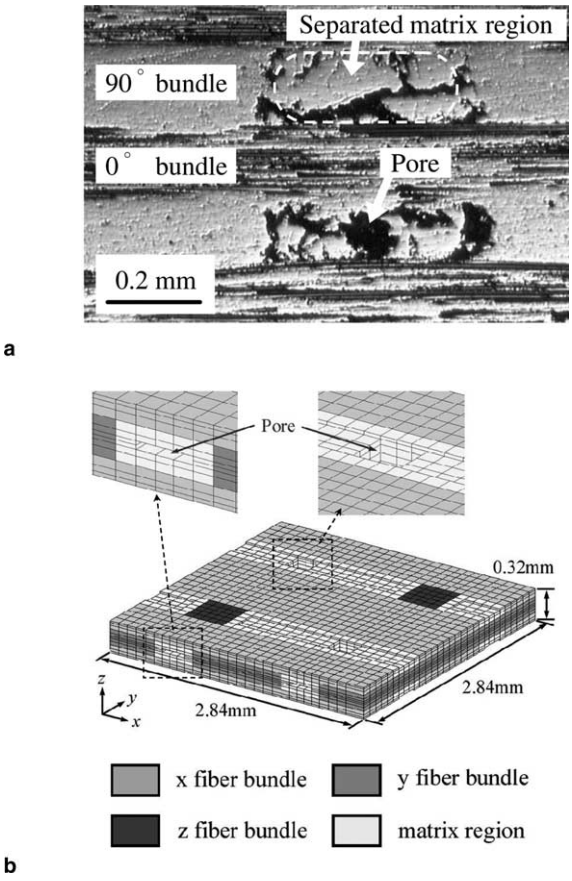

Fig. 9. Finite element model of an orthogonal 3D woven SiC/SiC composite. The pocket region (matrix region) was assumed to be pore. (a) Optical micrograph showing SiC matrix in pocket regions, (b) finite element model of the unit cell.

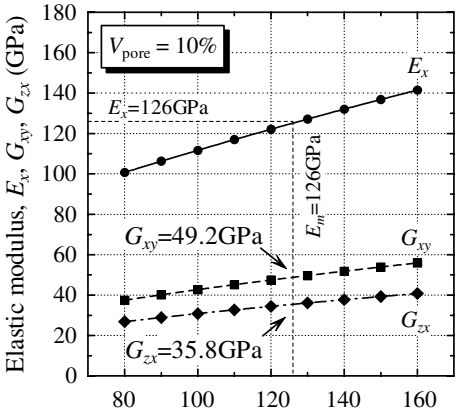

Fig. 10. Estimation of elastic moduli E_x, G_{xy}, and G_{zx} of the composite as a function of Young's modulus of matrix E_m.

4.3. Effect of on-axis tensile stress on shear properties

The relationship between torsional rigidity and on-axial maximum tensile stress is shown in Fig. 11.

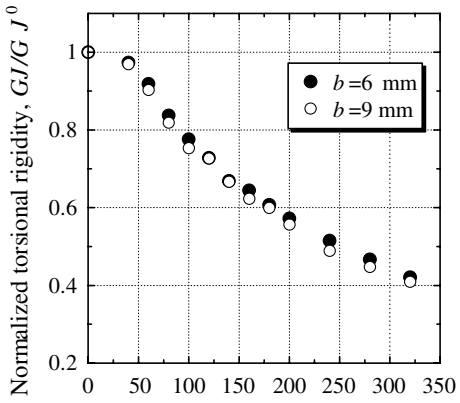

Fig. 11. Effect of on-axis tensile stress on torsional rigidity GJ. The torsional rigidity was normalized by the initial values of GJ_0.

The torsional rigidity GJ is normalized by the initial value GJ_0. The ultimate tensile strength was 414 MPa for a 6 mm width specimen, and 428 MPa for a 9 mm width specimen, respectively. The torsional rigidity values were measured up to on-axis stress levels of 320 MPa. Because the torsion moment versus twist angle relation was linear, it is suggested that any crack propagation did not occur during the torsional tests. The torsional rigidity finally decreased by 60% of the initial value at 320 MPa as shown in Fig. 11.

Degradation of the torsional rigidity indicates that shear moduli G_{xy} and G_{zx} vary due to on-axis tensile stress. The relationship between shear moduli and on-axis tensile stress is shown in Fig. 12, which represents the decrease of both G_{xy} and G_{zx}. As reported in the previous study [9], SiC/SiC woven composites suffer from two major damage modes under tensile stress: (1) transverse cracking in the transverse (90°) fiber bundles, and (2) matrix cracking in the longitudinal (0°) fiber bundles. An optical micrograph of the replica films, illustrating transverse cracking within the 90° fiber bundles and matrix cracking in the 0° fiber bundles at

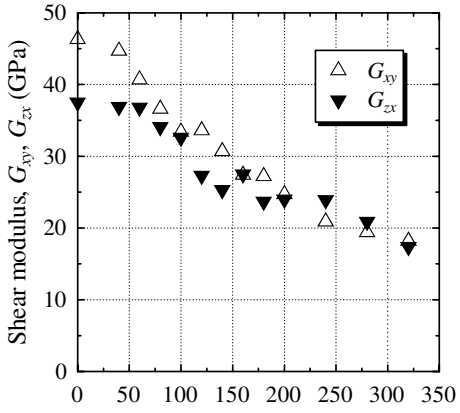

Fig. 12. The relationship between shear moduli (G_{xy}, G_{zx}) and on-axis tensile stress.

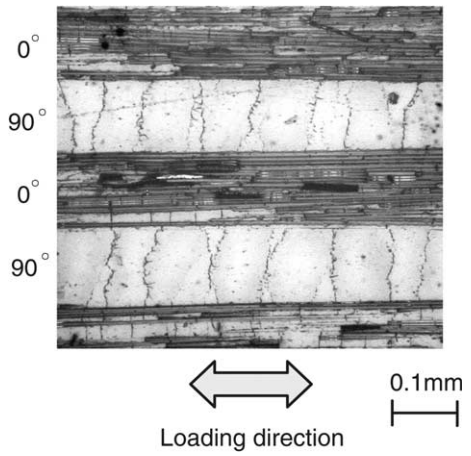

Fig. 13. Optical micrograph of the replica films, illustrating matrix cracking within the transverse (90°) fiber bundles at 320 MPa.

320 MPa, is shown in Fig. 13. Beyerle et al. [4] reported that the shear stiffness decreased under pure shear stress (Iosipescu shear test). The experimental results suggest that the shear stiffness degradation is caused by on-axis tensile stress as well as shear stress, and this is due to transverse cracking in 90° fiber bundles and matrix cracking in the 0° fiber bundles.

The relationship between the transverse crack density and maximum tensile stress is represented in Fig. 14. The onset of transverse crack propagation is approximately 40 MPa. The transverse crack initiation stress corresponds to the onset of decrease in GJ (see Fig. 11), and the crack density reaches 11–12 mm^{-1} at 320 MPa. From Fig. 12, it is seen that the tensile stress at the onset of decrease of G_{xy} coincides with the transverse crack initiation stress (40 MPa), whereas almost no degradation of G_{zx} is recognized until the tensile stress of 100 MPa. In laminated composites, it is well known that in-plane shear modulus degrades due to

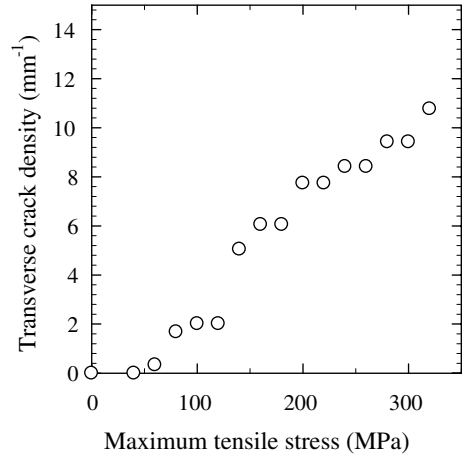

Fig. 14. Transverse crack density in the 90° fiber bundles as a function of the on-axis maximum tensile stress.

transverse cracking. However, Whitney [22] reported that out-of-plane shear modulus G_{zx} is insensitive to transverse cracking in 90° layers. These results indicate that G_{xy} decreases due to the accumulation of transverse cracks in the 90° fiber bundles and matrix cracks in the 0° fiber bundles, while G_{zx} is affected only by matrix cracks in 0° fiber bundles.

Finally, the degradation of in-plane shear stiffness of the orthogonal 3 D woven CMC as a function of transverse crack density is predicted using the shear-lag model. It is assumed that: (1) z-bundles are neglected here because of their low volume fraction, and orthogonal 3D woven composites are treated as laminates with multiple 0°/90° ply blocks (i.e., $([0°/90°]_s)_n$ laminates), and (2) analysis of $[0°/90°]_s$ laminates can be applied to $([0°/90°]_s)_n$ laminates. Fig. 15 shows schematic drawing of the shear-lag model of a cross-ply laminated composite. The relationship between the shear stresses and the through-the-thickness average in-plane displacements of each layer is written by the following equation:

$$\begin{bmatrix} \tau_{xz} \\ \tau_{yz} \end{bmatrix} = \begin{bmatrix} H_{11} & 0 \\ 0 & H_{22} \end{bmatrix} \begin{bmatrix} u_2 - u_1 \\ v_2 - v_1 \end{bmatrix}, \tag{6}$$

where u_i and v_i are average in-plane displacements of the 0° ($i = 1$) and 90° ($i = 2$) layers in the x and y directions. H_{11} and H_{22} are the shear-lag parameters. The shear-lag parameters are often dealt with as empirical parameters. The parameters are also determined by assuming the function of displacement (u_i, v_i) in each layer. For example, Tsai and Daniel [11], Nuismer and Tan [23] proposed the following equations as the shear-lag parameters:

$$H_{11} = \frac{3G_{LT}G_{TT}}{t_2 G_{LT} + t_1 G_{TT}}, \quad H_{22} = \frac{3G_{LT}G_{TT}}{t_1 G_{LT} + t_2 G_{TT}}, \tag{7}$$

where G_{LT} and G_{TT} are longitudinal and transverse shear stiffness of unidirectional composites (or fiber bundles), respectively, and t_1 and t_2 are thickness of 0° and 90° layers. The in-plane shear modulus of the whole laminate as a function of transverse crack density ρ is given by:

$$\frac{G_{xy}(\rho)}{G_{xy0}} = \left(1 + \frac{t_2}{t_1}\frac{2\rho}{\alpha}\tanh\left(\frac{\alpha}{2\rho}\right)\right)^{-1},$$
$$\alpha = \sqrt{\frac{H_{22}}{G_{LT}}\left(\frac{1}{t_1} + \frac{1}{t_2}\right)}. \tag{8}$$

When Eq. (7) is used for the shear-lag parameter, Eq. (8) predicts the lower limit of the shear stiffness reduction [12].

Using Eqs. (7) and (8) the in-plane shear modulus was calculated as a function of transverse crack density. The numerical result is plotted by the solid line in Fig. 16. The parameters used for the calculation were $G_{LT} = 45.3$ GPa, $G_{TT} = 29.3$ GPa and $t_1 = t_2 = 0.16$ mm, respectively. The shear moduli, G_{LT}, G_{TT}, of a lamina were assumed by the Reuss type approximation based on the experimental results. The effect of the 3D woven architecture including voids (pocket region) was not explicitly considered as described above, and incorporated into these shear modulus values. Although it is known that Eq. (8) predicts the lower limit, the numerical curve almost agreed with the experimental data. This result also suggests that the in-plane shear stiffness is degraded by matrix cracking in 0° fiber bundles as well as transverse cracking in 90° fiber bundles.

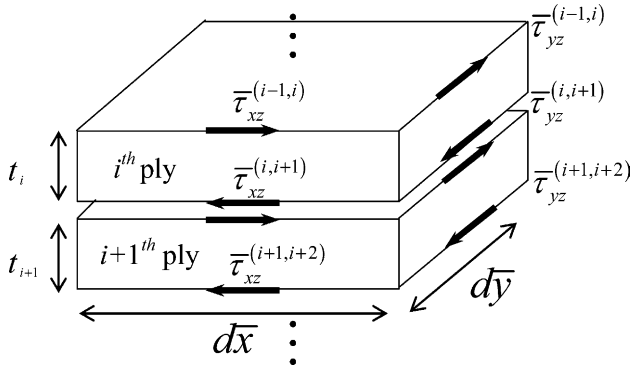

Fig. 15. Schematic drawing of a shear-lag model of a cross-ply laminated composite.

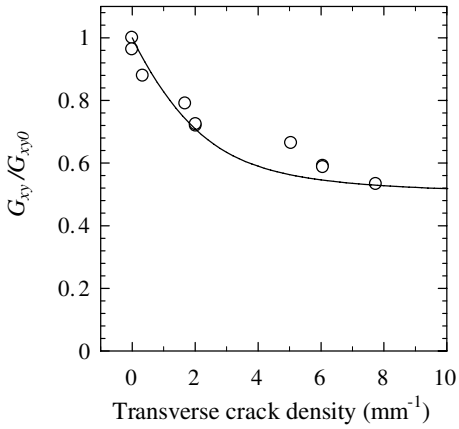

Fig. 16. Relationship between the shear modulus (G_{xy}) and the transverse crack density. Each shear modulus is normalized by the corresponding initial value (G_{xy0}).

5. Conclusion

Shear moduli G_{xy} and G_{zx} of an orthogonal 3D woven SiC/SiC composite were estimated by torsional tests of rectangular cross-section specimens. In-plane shear modulus G_{xy} from the torsional test agreed with that measured from ±45° off-axis tensile test. FEM

analysis based on homogenization method was also conducted for verifying the experimental results. A good correspondence between the analytical and the experimental results was obtained. The effect of on-axis tensile stress on shear properties was also investigated. Both in-plane and out-of-plane shear moduli decreased with increasing maximum tensile stress. It was confirmed that in-plane shear stiffness degrades due to transverse cracking in 90° fiber bundles and matrix cracking in 0° fiber bundles, while out-of-plane shear stiffness is affected by matrix cracking in 0° fiber bundles. The degradation of in-plane shear modulus was predicted based on the shear-lag model for a cross-ply laminated composite, and compared with experimental results.

It was demonstrated that the torsional test is an effective method to estimate out-of-plane shear modulus of ceramic matrix composites, because a thick specimen is not required.

References

[1] Evans AG, Zok FW. The physics and mechanics of fibre-reinforced brittle matrix composites. J Mater Sci 1994;29:3857–96.

[2] Hutchinson JW, Jensen HM. Models of fiber debonding and pullout in brittle composites with friction. Mech Mater 1990;9:139–63.

[3] Karandikar P, Chou T-W. Characterization and modeling of microcracking and elastic modulo changes in Nicalon/CAS composites. Comp Sci Technol 1993;46:253–63.

[4] Beyerle DS, Spearing SM, Evans AG. Damage mechanisms and the mechanical properties of laminated 0/90 ceramic/matrix composite. J Am Ceram Soc 1992;75(12):3321–30.

[5] Okabe T, Komotori J, Shimizu M, Takeda N. Mechanical behavior of sic fiber reinforced brittle-matrix composites. J Mater Sci 1999;34:3405–12.

[6] Kuo W-S, Chou T-W. Multiple cracking of unidirectional and cross-ply ceramic matrix composites. J Am Ceram Soc 1995;78(3):745–55.

[7] Xia ZC, Carr RR, Hutchinson JW. Transverse cracking in fiber-reinforced brittle matrix, cross-ply laminates. Acta Metall Mater 1993;41(8):2365–76.

[8] Park CH, McManus HL. Thermally induced damage in composite laminates: predictive methodology and experimental investigation. Comp Sci Technol 1996;56:1209–19.

[9] Ogasawara T, Ishikawa T, Ito H, Watanabe N, Davies IJ. Multiple cracking and tensile behavior for an orthogonal 3-D woven Si–Ti–C–O fiber/Si–Ti–C–O matrix composite. J Am Ceram Soc 2001;84(7):1565–74.

[10] Kobayashi S, Kawamoto H, Wakayama S. Evaluation of shear modulus of composite laminates containing microscopic damages. Mater Syst 2002;20:125–30 [in Japanese].

[11] Tsai CL, Daniel IM. The behavior of cracked cross-ply composite laminates under shear loading. Int J Solids Struct 1992;29(24):3251–67.

[12] Hashin Z. Analysis of cracked laminates: a variational approach. Mech Mater 1985;4:121–36.

[13] Gudmundson P, Zang W. An analysis model for thermoelastic properties of composite laminates containing transverse matrix cracks. Int J Solids Struct 1993;30:3211–31.

[14] Cady C, Heredia FE, Evans AG. In-plane mechanical properties of several ceramic-matrix composites. J Am Ceram Soc 1995;78(8):2065–78.

[15] Genin GM, Hutchinson JW. Composite laminates in plane stress: constitutive modeling and stress redistribution due to matrix cracking. J Am Ceram Soc 1997;80(5):1245–55.

[16] Ishikawa T, Koyama K, Kobayashi S. Elastic moduli of carbon-epoxy composites and carbon fibers. J Compos Mater 1977;11:332–44.

[17] Lekhnitskii SG. Theory of elasticity of an anisotropic elastic body. San Francisco: Holden-Day, Inc.; 1963. p. 197–205.

[18] Tsai C-L, Daniel IM, Yaniv G. Torsional response of rectangular composite laminates. J Appl Mech 1990;57:383–7.

[19] Swanson SR. Torsion of laminated rectangular rods. Comput Struct 1998;42:23–31.

[20] Ishikawa T, Bansaku K, Watanabe N, Nomura Y, Shibuya M, Hirokawa T. Experimental stress/strain behavior of SiC-matrix composites reinforced with Si–Ti–C–O fibers and estimation of matrix elastic modulus. Comp Sci Technol 1998;58:51–63.

[21] Watanabe N, Teranishi K. Thermal stress analysis for Al honeycomb sandwich plates with very thin CFRP faces. AIAA-95-1394; 1995.

[22] Whitney JM. Effective elastic constants of bidirectional laminates containing transverse ply cracks. J Comp Mater 2000;34:954–78.

[23] Nuismer RJ, Tan SC. Constitutive relations of a cracked composite lamina. J Comp Mater 1989;22:306–21.